Design of High Performance Graphene/Silicon Photodetectors

Saqib Iqbal
Department of Electrical Engineering
Lahore University of Management Sciences (LUMS)
Lahore, Pakistan
15060005@lums.edu.pk

Hassan Imran, Usama B. Qasim and Nauman Z. Butt
Department of Electrical Engineering
Lahore University of Management Sciences (LUMS)
Lahore, Pakistan
15060064@lums.edu.pk 15060059@lums.edu.pk
nauman.butt@lums.edu.pk

***Abstract*—A thin layer of graphene on a light absorbing substrate (*e.g.,* Silicon (Si)) is capable of an ultrahigh sensitivity for light detection. Demonstrated in both 2 terminal (diode) and 3 terminal (MOSFET) configurations, graphene on *Si* devices can outperform conventional photodetectors in detecting weak light signals. High photo responsivity in graphene on *Si* originates from substrate a combined effect of (i) graphene doping due to photo generated carrier injection from substrate, and, (ii) high carrier mobility of graphene which enable a large quantum gain. Here we explore the design parameters that affect the photo induced graphene doping using self-consistent numerical simulations. We note that photo response can be substantially improved when substrate carriers have low mobility and high lifetime. The apparently counter-intuitive dependence of photo response on substrate's mobility is physically explained.**

Keywords—photodetectors; silicon; graphene; responsivity; quantum gain;

I. INTRODUCTION

Graphene is a two dimensional mono atomic layer material which have demonstrated remarkable electronic and optoelectronic properties [1-4], in particular, a very high carrier mobility (200,000 $cm^2V^{-1}S^{-1}$ at room temperature) [5, 6]. A single layer graphene can be termed as a semiconductor with zero bandgap or a semi-metal with tunable Fermi level [7, 8]. Due to these extraordinary attributes, Schottky junctions made between graphene and conventional semiconductors have exhibited unique applications for a variety of devices [9]. In particular, graphene-silicon junctions have found a huge interest for solar cells and photodetectors due to an easy integration of graphene with silicon [10, 11]. Other examples of such junctions include gas sensors [12], optical modulator [13], and, the barrister [14]. In particular, highly sensitive photodetectors based on graphene on silicon (GoS) have demonstrated a remarkably high photoresponsivity (R) in various types of device configurations [15]. The quantitative modeling and simulations based design optimizations of GoS photodetectors have however been relatively less explored despite several experimental demonstrations of impressive photoresponsivity (R).

In the existing models, the physical origin of photo response in GoS is described by: (i) Quantum carrier reinvestment (QCR) model [16], and, (ii) substrate induced doping of graphene [17].

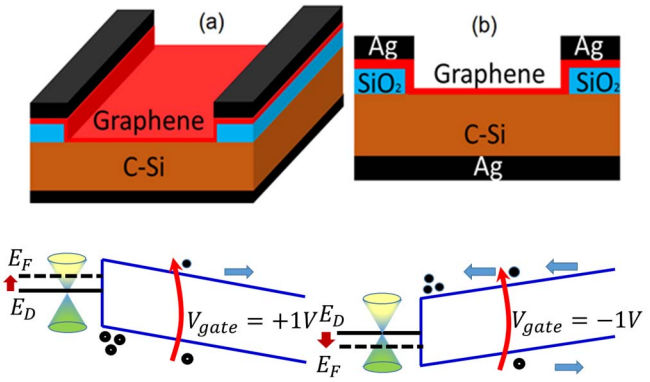

Fig. 1 (a) Three dimensional (*3-D*) illustration of Si/Graphene photodetector (b) *2-D* cross section of the device model in this work. Crystalline silicon (c-Si) acts as photo absorbing material, while single layer graphene forms the channel between source and drain. Energy band diagram along the direction perpendicular to graphene channel for two different back gate voltages ($V_{bg} = \pm 1\ V$). The photogenerated carriers inside Si are transferred into graphene depending upon the applied V_{bg}. The electrostatic potential of graphene is modulated due to low quantum capacitance (C_q) of two dimensional graphene.

In QCR model, the photocurrent (J_{photo}) in GoS is directly calculated from quantum gain (QG) is defined by: $QG = QE \times \tau/\tau_t$, where QE is the quantum efficiency, and, τ_t is the carrier transit time in graphene. The effect of conduction modulation in graphene due to its doping variation induced by substrate's carrier injection is not quantitatively modeled in this approach. In the 2nd model, the role of graphene doping is explicitly considered but so far only the photo-induced electrostatic field effect of substrate's photo generated carriers has been modeled while the physical carrier injection from substrate to graphene has never been simulated. In this paper, we develop a comprehensive approach which not only incorporates both of the existing models but also include the effect of self-consistent carrier transport from substrate to graphene to accurately predict the photoresponse of GoS photodetectors. This paper is divided in four sections. Section II describes the device modeling approach and simulation details. Section III discusses the results and conclusions are presented in section IV.

© 2017 The Japan Society of Applied Physics

II. Device Modeling Approach

A three dimensional (3−D) illustration and 2−D cross section of the investigated device is shown in Fig. 1(a) and 1(b) respectively. The structure is a field-effect phototransistor, in which graphene forms the channel that is back gated through an intrinsic (undoped) silicon (Si) substrate and is contacted at the top by source/drain metal.

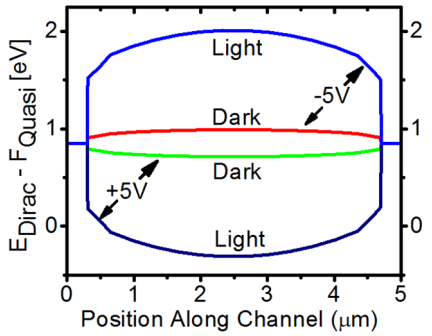

Fig. 2. Change in graphene potential $E_{Dirac} - F_{Quasi}$ along the channel under dark and illumination for different V_{bg}. Under illumination, the photogenerated carriers are transferred into graphene and graphene potential is modulated.

The model is independent from any specific process/deposition method of graphene. The interfacial properties non-idealities such as presence of defects or a native oxide (which are process dependent) are ignored to focus on the first order mechanisms.

The energy band diagram along the direction perpendicular to the graphene channel for back gate voltage $V_{bg} = \pm 1\,V$ is shown in Fig. 1(c) and 1(d). The photogenerated electrons or holes are transferred into graphene depending upon the polarity of V_{bg}. The transferred carriers modulate the graphene potential due to smaller quantum capacitance ($C_{q,grp}$) of graphene that depends upon the density of states of graphene. $C_{q,grp}$ can be approximated by [17]:

$$C_{q,grp} = \beta q^2 \left[2k_B T \cdot ln\left(1 + e^{\mu/k_B T}\right) - \mu\right]$$

Where β is material constant ($\beta = 1.5 \times 10^6 \mu m^{-2} eV^{-2}$) and μ is the Fermi level with respect to Dirac point. It is worth noting that $C_{q,grp}$ is the function of μ and, hence, depends upon the work function (doping) of graphene.

The electrostatic doping modulates the graphene resistance (R_{grp}) and given by [18]:

$$R_{grp} = \alpha \left[\left(\frac{2q^2}{h}\right)\frac{2\lambda}{\pi\hbar v_F}\frac{W}{L}(k_B T)(s+1)^2 \Gamma\left(F_s(\eta_F) + F_s(-\eta_F)\right)\right]^{-1}$$

where Γ is the gamma function, F_s is the Fermi–Dirac integral of order s, $\eta_F = (E_D - EF)/k_B T$, and λ is the mean free path of the carriers in the graphene [17, 18]. The pre factor $\alpha \geq 1$ captures the effect of sub unity transmission probability between the source/drain metal and the underlying graphene [17].

The device under observation is solved numerically using a 2−D simulation tool Padre [ref] which solves the coupled set of Poisson and drift-diffusion equation self-consistently. The Poisson equation is given by:

$$\nabla^2 V(x) = \frac{q}{\epsilon}[N_D^+ - N_A^- + p(x) - n(x)]$$

where q is charge on electron, ϵ is permittivity of the absorber, N_D^+ (N_A^-) are donor (acceptor) concentration, $p(x)$ and $n(x)$ are position dependent hole and electron concentration respectively. The continuity equation for electrons is given by:

$$\frac{\partial n}{\partial t} = \frac{1}{q}\nabla \cdot J_n + G(x) - R(x)$$

where J_n is electron current density, $G(x)$ and $R(x)$ are carrier generation and recombination rates respectively. The drift-diffusion equation for electrons is given by:

$$J_n = qn\mu_n \frac{dV(x)}{dx} + qD_n \frac{dn}{dx}$$

where μ_n is the mobility of electron and D_n is the diffusion constant for electrons respectively.

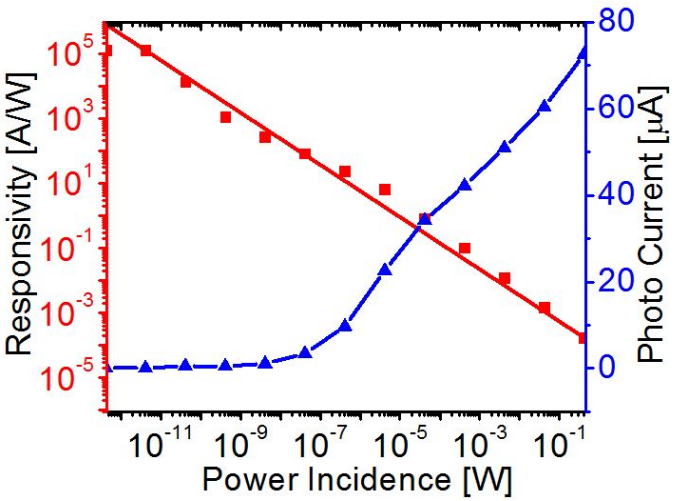

Fig. 3. Responsivity (R) and photocurrent (I_{photo}) as a function of incident photon power (P_{inc}). The photodetector exhibits a high R ($\approx 10^5 A/W$) for P_{inc} ($\approx 10^{-12}\,W$). The red line shows the power law fit ($R \propto P_{inc}^{\alpha}$) for the simulated data with $\alpha = -0.80$.

III. Results and Discussion

The change in graphene potential ($E_{Dirac} - F_{Quasi}$) along the channel for different V_{bg} under dark and illumination is shown in Fig. 2. Under illumination, the photo generated carriers are transferred into graphene and the graphene potential is modulated. Under illumination, $E_{Dirac} - F_{Quasi}$ is much higher as compared to that of dark. The responsivity (R) and photocurrent (I_{photo}) of the photodetector as a function of incident photon power (P_{inc}) is shown in Fig. 3. The photodetector exhibits a high R ($\approx 10^5\,A/W$) for P_{inc} as low as $10^{-12}\,W$. The red line shows the power law fit ($R \propto P_{inc}^{\alpha}$)

for the simulated data with $\alpha = -0.83$. Fig. 4(a) shows the I_{photo} as a function of V_{bg} for a range of carriers mobility in silicon. It is important to note that a lower μ results into a higher I_{photo}, an observation which is contrary to the intuition since drift length (l_{drift}) is proportional to μ and given by $l_{drift} = \mu \times \tau \times \varepsilon$.

We however note that the l_{drift} for carriers in substrate is high enough for the given range of μ due to V_{bg} and a relatively high τ for c-Si. So, recombination in Si is negligible implying 100% carrier collection efficiency. Since injected I_{photo} is constant in this case, a lower μ results in a higher density of carriers at Si/graphene interface and hence a higher graphene doping to lower the R_g and hence, I_{photo} is enhanced. Fig. 4(b) represents the $Iphoto$ as a function of Vbg for a range of carriers lifetime in silicon. For higher τ, more number of photo generated carriers are transferred into graphene to modulate the graphene potential that results in higher graphene doping. High graphene doping lowers the graphene resistance and hence $Iphoto$ increases. The comparison of R and $Iphoto$ as a function of $Pinc$ for the modeled device vs the experimental data of [2] is shown in Fig. 5(a) and 5(b) respectively.

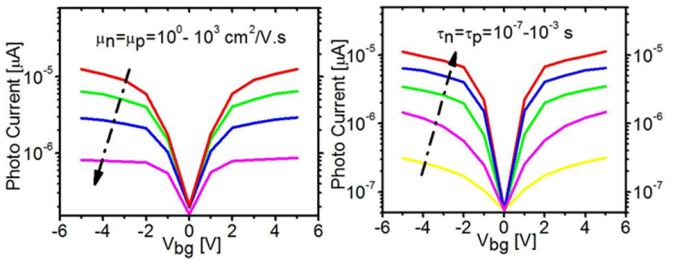

Fig. 4. I_{photo} as a function V_{bg} for different carrier mobility in silicon. For lower μ, more number of photogenerated carriers (n) are transferred into graphene to keep injected I_{photo} $(= Aqn\mu_n\varepsilon)$ constant, and hence results in higher graphene doping. I_{photo} as a function V_{bg} for different carrier lifetime in silicon. For higher τ, more number of photogenerated carriers (n) are transferred into graphene to modulate graphene resistance, and hence results in higher I_{photo}.

The Si/graphene photodetector exhibits a good match with experimental data of [2] for both R and $Iphoto$. Fig. 5(c) shows the comparison of $Iphoto$ as a function of wavelength (λ) for modeled device vs experimental data of [2]. A high $Iphoto$ is achieved for higher energy photons due to higher absorption in silicon due to higher absorption coefficient (α) for such photons. For low energy photons, $Iphoto$ drops significantly due to lower absorption in Si and hence lesser number of carriers can transfer into graphene to modulate $Rgrp$. Fig. 5(d) shows the comparison of $Iphoto$ as a function of source/drain voltage (Vds) for the modeled device vs experimental data of [2]. $Iphoto$ increases linearly with Vds due to higher electric field (ε) between source and drain for higher Vds. The high ε, hence, increases the carriers drift length ($ldrift$) and more number of carriers can flow between source and drain, and hence, I_{photo} is increased.

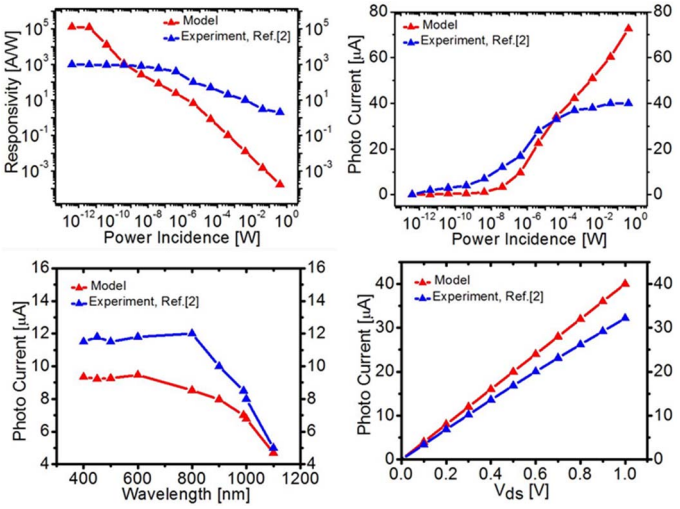

Fig. 5 (a) Comparison of R as a function P_{inc} for modeled device vs experimental data of [2]. (b) Comparison of I_{photo} as a funciton of P_{inc} for modeled device vs experimental data of [2]. The Fig. shows a good match of R and I_{photo} with the experiment. Comparison of I_{photo} as a function wavelength (λ) for modeled device vs experimental data of [2]. A high I_{photo} is achieved for higher energy photons due to higher absorption in silicon. For low energy photons, I_{photo} drops significantly due to lower absorption in Si and hence lesser number of carriers can transfer into graphene. Comparison of I_{photo} as a function source/drain voltage (V_{ds}) for modeled device vs experimental data of [2]. As V_{ds} is increased, I_{photo} increases linearly due to larger dirft length (l_{drift}) of carries inside graphene that can transfer into source/drain metal and high I_{photo} is achieved.

IV. Conclusion

We show that the photoresponse of GoS photodetectors can be effectively improved through optimizing the substrate material properties. Our computational approach allows incorporating the photo induced graphene doping model as well as the quantum gain model in a self-consistent unified model. The graphene/Si photodetector exhibits a high responsivity of 10^5 A/W for power incident of 10^{-12} W. High carrier lifetime in Si is required to attain a high photocurrent. A lower carrier mobility in silicon results in higher accumulation of photogenerated carriers near graphene/silicon interface which increases the electrostatic doping in the graphene channel. A lower carrier mobility in substrate therefore provides a high photocurrent and photoresponsivity. A high photoresponsivity is maintained for a relatively broad range of wavelength conforming to trends observed in the experiments.

ACKNOWLEDGMENT

The authors would like to thank H. Ullah for fruitful discussion. They would also like to thank I. Z. Durrani and A. Farooq for their valuable suggestions and comments to improve the quality of work.

REFERENCES

1. Schwierz, F., *Graphene transistors.* Nature nanotechnology, 2010. **5**(7): p. 487-496.
2. Guo, X., et al., *High-performance graphene photodetector using interfacial gating.* Optica, 2016. **3**(10): p. 1066-1070.
3. Neto, A.C., et al., *The electronic properties of graphene.* Reviews of modern physics, 2009. **81**(1): p. 109.
4. Geim, A.K. and K.S. Novoselov, *The rise of graphene.* Nature materials, 2007. **6**(3): p. 183-191.
5. Bolotin, K.I., et al., *Ultrahigh electron mobility in suspended graphene.* Solid State Communications, 2008. **146**(9): p. 351-355.
6. Du, X., et al., *Approaching ballistic transport in suspended graphene.* Nature nanotechnology, 2008. **3**(8): p. 491-495.
7. Bao, Q. and K.P. Loh, *Graphene photonics, plasmonics, and broadband optoelectronic devices.* ACS nano, 2012. **6**(5): p. 3677-3694.
8. Vakil, A. and N. Engheta, *Transformation optics using graphene.* Science, 2011. **332**(6035): p. 1291-1294.
9. Li, X., et al., *Graphene-on-silicon Schottky junction solar cells.* Advanced Materials, 2010. **22**(25): p. 2743-2748.
10. Wang, X., et al., *High-responsivity graphene/silicon-heterostructure waveguide photodetectors.* Nature Photonics, 2013. **7**(11): p. 888-891.
11. An, X., et al., *Tunable graphene–silicon heterojunctions for ultrasensitive photodetection.* Nano letters, 2013. **13**(3): p. 909-916.
12. Singh, A., et al., *Tunable Reverse-Biased Graphene/Silicon Heterojunction Schottky Diode Sensor.* Small, 2014. **10**(8): p. 1555-1565.
13. Liu, M., et al., *A graphene-based broadband optical modulator.* Nature, 2011. **474**(7349): p. 64-67.
14. Yang, H., et al., *Graphene barristor, a triode device with a gate-controlled Schottky barrier.* Science, 2012. **336**(6085): p. 1140-1143.
15. Xia, F., et al., *Ultrafast graphene photodetector.* Nature nanotechnology, 2009. **4**(12): p. 839-843.
16. Liu, N., et al., *A pomegranate-inspired nanoscale design for large-volume-change lithium battery anodes.* Nature nanotechnology, 2014. **9**(3): p. 187-192.
17. Butt, N.Z., et al., *Substrate-Induced Photofield Effect in Graphene Phototransistors.* IEEE Transactions on Electron Devices, 2015. **62**(11): p. 3734-3741.
18. Lundstrom, M., T. Low, and D. Berdebes, *Low bias transport in graphene: an introduction (lecture notes).* 2009.